JOURNAL OF SOLID STATE CHEMISTRY 105, 313–335 (1993)

Order and Disorder in $(Nd,Ce)_nO_{2n}Sr_2GaCu_2O_5$ and $YSr_2CoCu_2O_7$

T. KREKELS, O. MILAT,* G. VAN TENDELOO, AND S. AMELINCKX

University of Antwerp (R.U.C.A.), Groenenborgerlaan 171, B-2020 Antwerp, Belgium

AND T. G. N. BABU, A. J. WRIGHT, AND C. GREAVES

School of Chemistry, University of Birmingham, Birmingham B15 2TT, England

Received November 9, 1992; accepted November 18, 1992

The structures of the compounds $YSr_2CoCu_2O_7$ and $(Nd/Ce)Sr_2GaCu_2O_5$ and $(Nd/Ce)_2Sr_2GaCu_2O_9$ $[(Nd/Ce)_nSr_2GaCu_2O_{5+2n}, n = 1, 2, \ldots]$ are considered as derivatives of the prototype 123-phase. They were previously found to contain layers of corner-sharing MO_4 tetrahedra. In this paper we describe the superstructures which consist of a regular alternation of the two types of symmetry related MO-chains leading to period doubling along the direction normal to the chains. These conclusions are based on electron diffraction and on direct image evidence from high resolution electron microscopy. Both compounds are fragmented in domains resulting from the two crystallographically equivalent orientations of the chains which differ by 90°. Both compounds contain linear defects confined to one MO-layer. Twin "lines" are due to orientation changes of the chains within a single MO-layer and antiphase boundary lines result from the parallel shift over one interchain distance, of two parts of a layer.

1. Introduction

Doping of superconducting materials by the isomorphous substitution of aliovalent ions, with the effects of these dopants on the superconducting properties studied, has proved to be one of the most successful methods in obtaining information on the structural requirements for the occurrence of high T_c superconductivity; it also allows the optimization of these properties (*1*).

It is surprising to what extent the $YBa_2Cu_3O_7$ (commonly called "123") compound is tolerant in accepting various substitutions without profoundly modifying its structural features (*2*, *3*), even though the superconducting properties are strongly influenced. In particular, a number of metallic dopants, which are incorporated preferentially or exclusively in the CuO-layer of the 123-structure, are found to affect profoundly the superconducting properties, in particular, the critical temperature.

One important conclusion of these experiments is the finding that the structural integrity of the CuO_2-layer seems to be crucial for the occurrence of superconductivity (*4*), but that the stoichiometry and the dopant atoms in the CuO-layer are important in determining the number and the type of charge carriers (*5*).

In the course of such experiments in various laboratories (*1–18*), a large number of compounds were prepared and their structures determined. Among these compounds those containing gallium and cobalt are of particular interest since they change the oxygen coordination in the GaO- or CoO-layer replacing the CuO-layer of the prototype 123-compound. The structures of these compounds have been studied by means of X-ray and neutron diffraction (*6–*

* On leave from Institute of Physics, University of Zagreb, Bijenicka 46, P.O. Box 304, 41000 Zagreb, Croatia.

0022-4596/93 $5.00

8), and it was shown that the oxygen coordination around these ions is tetrahedral, i.e., fundamentally different from the square planar configuration around copper.

The isostructural compounds $YSr_2Cu_2CoO_7$ (called "1212-Co" below) and $YSr_2Cu_2GaO_7$ (discussed in (*6*, *7*) and called "1212-Ga" below) are closely related to the prototype 123-compound. However, Co ions, as well as Ga ions, have a strong tendency to be tetrahedrally coordinated by oxygen ions. As a result, the *M* and O ions (*M* = Co or Ga, not Cu) of the *M*O-layer, which replaces the CuO-layer of the 123-compound, adopt a configuration consisting of chains of corner-sharing MO_4-tetrahedra, along the $[110]_p$ and $[1\bar{1}0]_p$ directions. (The subindex p denotes indexing relative to the perovskite base.) However, for the 1212-Co-compound, as well as for the 1212-Ga-compound, electron diffraction has revealed deviations from the structure proposed for the 1212-Ga-compound (*6*), leading to long range ordered superstructures.

It has also been shown previously that the rare-earth layer in the 123-compound can be replaced by a fluorite-like lamella of variable thickness (*9–15*). In the compound $(Nd,Ce)_nO_{2n}Sr_2GaCu_2O_5$ (referred to as "*n*212-Ga" below), the rare-earth layer was replaced by fluorite-like lamellae of $(Nd,Ce)O_2$ and at the same time the CuO-layer was replaced by a GaO-layer identical to the GaO-layer of the 1212-Ga-compound. We have studied the order and disorder phenomena introduced by the latter substitutions.

2. Synthesis and Characterization

The materials studied were synthesized using conventional solid state methods involving intimate stoichiometric mixtures of high purity Y_2O_3, $SrCO_3$, Co_3O_4, CuO, Nd_2O_3, CeO_2, and Ga_2O_3. Single phase $YSr_2CoCu_2O_7$ was obtained after three heat treatments in air (20 hr at 1000°C) with intermediate grinding. Samples of composition $(Nd_{1.5}Ce_{0.5}Sr_2GaCu_2O_{9\pm x}$ were prepared by firing twice for 12 hr at 1080°C in oxygen, but X-ray powder diffraction patterns indicated slight contamination (ca. 5%) with one or more unidentified impurities. The extent of contamination was monitored for samples with slightly different cation ratios, and the major cause of the impurities appeared to relate to the partial substitution of Nd on the Sr sites. Accordingly, samples with lower Sr and higher Nd contents were synthesized, and the composition $(Nd_{1.5}Ce_{0.5})(Sr_{1.8}Nd_{0.2})GaCu_2O_{9\pm x}$ was subsequently found to yield an essentially single phase product, which was used in the structural examinations reported here. The X-ray powder diffraction trace was indexed on an orthorhombic unit cell with dimensions $a = 5.527(3)$, $b = 5.462(3)$, and $c = 28.36(1)$ Å.

3. Structural Considerations

With the structure of the 123-compound achieving the status of a "prototype" or "reference" phase for a wide class of perovskite-derived layered cuprates, it seems meaningful to describe the structures under study by comparison with that of $YBa_2Cu_3O_7$ (*19*, *20*). In $YBa_2Cu_3O_7$ the succession of the layers along the *c*-direction is

. . .–CuO–BaO–CuO_2–
Y–CuO_2–BaO–. . . .

The structure is orthorhombic, pseudotetragonal with $a_p \approx b_p \approx 0.38$, $c_p = 1.17$ nm.

The replacement of barium either by strontium or by a mixture of strontium and cerium to obtain the 1212-compounds, resp. the *n*212-compounds, does not change the topology of the structure. The Y-layer, which is oxygen free in the $YBa_2Cu_3O_7$-structure, is replaced by a fluorite-like lamella of $(Nd,Ce)O_2$ in the *n*212-compound. This type of substitution has been described before (*9*) for other perovskites and it was shown that, e.g., in the compounds with composition $(Y,Ce)_nSr_2Cu_2(Cu,Fe)O_{4+2n+z}$ ($z = 1$), the fluorite-like block, which con-

sists in this case of $(Y,Ce)_nO_{2n}$, may contain one, two, three, or more layers. These compounds thus form a homologous series of mixed layer compounds with n = 1, 2, 3, . . . (*13*, *14*, *15*). The different compounds can be distinguished by their c-parameters which obviously increase with the number of such layers. The c-parameter of the three homologous phases with one, two, and three fluorite-like layers are respectively: c_1 = 2.28 (= 2 × 1.14), c_2 = 2.82, and c_3 = 3.36 nm. The thickness of a triple perovskite block, containing the succession of layers . . .–*M*O–SrO–CuO_2–(Nd/Ce)–CuO_2–SrO–. . . is 1.14 nm. The thickness-increment due to the addition of one (Nd/Ce)O_2-layer in a lamella is thus c_F = 0.27 nm. Moreover, every additional (more than a single) layer induces a shift of the perovskite blocks on both sides of the fluorite-like lamella over $\frac{1}{2}[110]_p$. Thus, if this number of layers is odd successive perovskite blocks are vertically aligned along the c-direction. With an even number of layers the perovskite blocks on both sides of the fluorite-like lamellae are shifted one relative to the other over $\frac{1}{2}[110]_p$. As a result the lattice becomes body-centered and the c-parameter doubles.

The former substitutions leave the main features of the triperovskite structure unchanged and, in particular, the tetragonal symmetry of the perovskite block is conserved. This is no longer the case when the CuO-layer of the 123-compound is replaced by an *M*O-layer (*M* = Co or Ga), since the preferred configuration of oxygen around Ga or Co is different from that around copper.

The square planar configuration of oxygen around copper, which gives rise to the –Cu–O–Cu– chains in the 123-compound, is replaced by a deformed tetrahedral configuration of oxygen around the *M* ions. The tetrahedron of oxygen atoms around the *M* ion consists of the two oxygen atoms of the SrO-layer, forming the apexes of the CuO_5-pyramid, and of two oxygen atoms in the *M*O-layer. The formation of the tetrahedra gives rise to chains of corner-linked tetrahedra along the $[110]_p$ directions, separated by channels of oxygen vacancies along the same directions. The CuO-layer of the 123-compounds is compared with an idealized *M*O-layer model of the studied compound in Fig. 1. Formally the MO_4 tetrahedra can be generated, starting from the square planar CuO-configuration by dis-

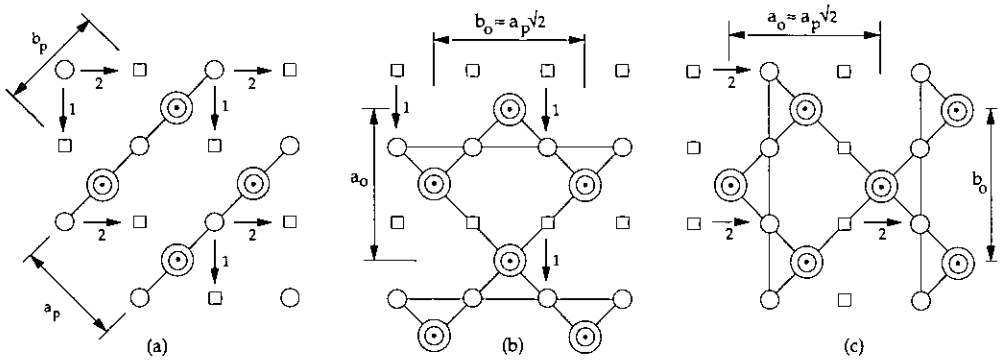

FIG. 1. Schematic representation of the formation of chains of corner-linked tetrahedra in *M*O-layers with reference to the square planar configuration present in CuO-layers (small circles are oxygen atoms, large circles *M* atoms, circles in heavy lines are apical SrO-plane oxygen atoms, squares are oxygen vacancies, dots are Cu-positions), (a) Square planar configuration of oxygen around copper (represented by a black dot); vacancies are represented by squares. Two possible atom displacements leading to tetrahedron formation are indicated by two sets of arrows; (b) the chains of tetrahedra have been formed along the horizontal direction by the atom displacements 1; (c) the chains of tetrahedra have been formed along the vertical direction by the atom displacements marked 2; The configurations have been idealized to emphasize the relationship with the basic perovskite structure.

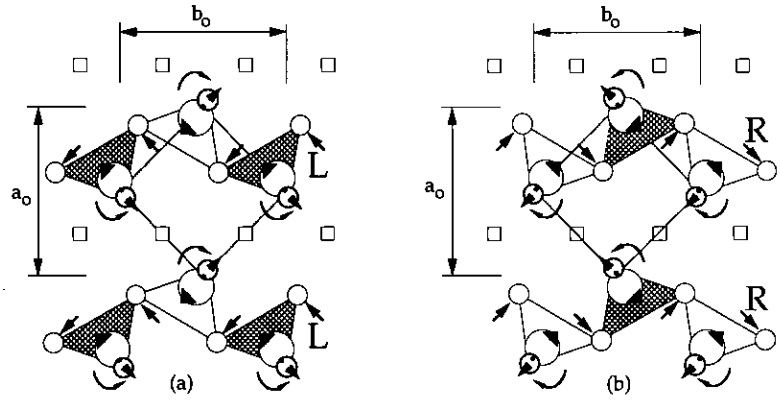

FIG. 2. The M–O-separation is increased by the rotation of the tetrahedra. The rotations can take place in two different senses. (a) A "left" L-chain is generated; (b) a "right" R-chain is generated. Tetrahedra rotated in positive sense are filled, rotation directions are indicated by circular arrows, oxygen atom displacements by straight arrows, metal displacements by heavy arrows. (a) All atoms in the MO-plane have a displacement vector component pointing to the left; (b) all displacement vectors have a component to the right.

placing oxygen atoms into vacant positions in the CuO-layer as indicated schematically in Fig. 1. Depending on the assumed displacements, indicated as 1 or 2, the resulting chains of MO_4 tetrahedra will all be oriented along $[110]_p$, or all along the perpendicular direction $[1\bar{1}0]_p$.

This idealized configuration will not be realized in practice, but the chain, represented in Fig. 2, will form instead (*6*). This is a consequence of the fact that the M–O-separation in the plane is too small in the idealized configuration; the M–O-distance increases when the oxygen atoms move toward the oxygen vacancy channels, as indicated by straight arrows in Figs. 2a and 2b The tetrahedra are hereby rotated about an axis parallel to c. The M-atoms will leave the original Cu-position, moving slightly toward the center of the tetrahedron. The corner-linking causes successive tetrahedra (along $[110]_p$ or $[1\bar{1}0]_p$) to be rotated in opposite sense.

It is important to note that the rotations can take place in two a priori equally probable senses giving rise to zigzag chains of opposite "phase" as represented in Fig. 2. We shall call such parallel chains left (L) and right (R) (*23*). In the structure formerly proposed for the 1212-Ga-compound and considered as the basic structure (indexes refering to it having subindex o) (*6*), either all chains are L-chains or all chains are R-chains.

The basic undistorted unit cell with all chains parallel and of the same type acquires a rectangular quasi-square mesh, diagonal relative to the perovskite mesh ($a_o \approx b_o = \sqrt{2}a_p$), in the $(001)_p$ plane. The a_o or $[100]_o$ direction is chosen perpendicular to the chains, the b_o or $[010]_o$ direction parallel to the chains (Fig. 2). Cell parameters are $a_o = 0.54$, $b_o = 0.55$ nm for the n212-Ga-compound; $a_o \approx b_o = 0.54$ nm for the 1212-Co-compound. In both the compounds studied, the chains are parallel in two successive MO-layers and are shifted with respect to each other in such a way that they form a staggered arrangement when they are viewed end on. For the 1212-compound or n212-compound with odd n, this shift over $[100]_p$ (or equivalently $[010]_p$) or $\frac{1}{2}$ $[110]_o$ causes a centering of the lattice and a doubling of the c-parameter: $c_o = 2c_p$. The space group proposed for the 1212-Ga-compound is $Ic2m$ (*6*, *8*). For the n212-compound with n even, the shift of the MO-layers over $\frac{1}{2}$ $[110]_p$ or $\frac{1}{2}$ $[100]_o$ results from

the shift between the perovskite blocks, due to the presence of the fluorite-like layer. The structure becomes B-face centered orthorhombic (quasi-tetragonal) with lattice parameters $a_o \approx b_o \approx \sqrt{2}a_p$; $c_o = 2c_p + n \cdot c_F$. In the model proposed in (6) all chains were assumed to be identical (L or R). In this paper we propose an orthorhombic superstructure in which these "chain-sites" are occupied in an ordered way, alternatingly by L- and R-chains, leading to a doubling of the lattice parameter along the a_o direction: $a_s = 2a_o$; the other superlattice parameters remain unchanged: $b_s = b_o$; $c_s = c_o$.

The L–R distinction is only a relative distinction because an L-chain is transformed into an R-chain by a mirror operation perpendicular to the chain direction or by a rotation of 180° about the c-axis. Such a mirror is a symmetry plane for the tetragonal perovskite blocks between which the MO-layers are sandwiched. This means that the L and R-chains have identical surroundings and hence are energetically equivalent; both will thus be formed with equal probabilities.

The presence of an oxygen vacancy or of a square-planarly coordinated Cu ion may interrupt the corner-linking in the chain. Hence an L-chain may become an R-chain along the same line, at such a point defect (Fig. 3). Alternatively, the presence of a copper atom in an MO-chain may induce a change in direction by 90° of the MaO-chain by forming a square planar configuration of oxygen around the copper (Fig. 4). Disorder in the MO-layer can thus a priori be expected at several structural levels: An L-chain may change into an R-chain by the presence of a vacancy or copper atom, or it may change its orientation by 90° within the same layer; the L–R arrangement within the layers may exhibit deviations from a regular arrangement (such as . . .–L–R–L–R–. . .); finally, stacking disorder between successive MO-layers may exist. No such possibilities are present in any other layer. These considerations suggest that any disorder is most probably associated with the MO-layer; we shall present direct high resolution evidence that this is the case.

4. Diffraction Patterns

4.1. The 1212-Co-Compound

Monodomain diffraction patterns along the simple crystallographic zones $[001]_o$, $[010]_o$, $[100]_o$, and $[2\bar{1}0]_o$ (=$[1\bar{1}0]_s$) are re-

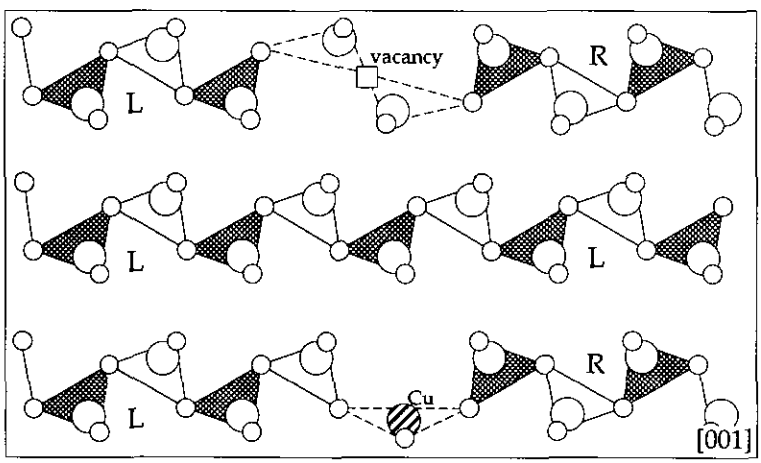

FIG. 3. Schematic drawing of MO-chains. The presence of a vacancy or of a copper atom may induce an L-chain to become an R-chain or vice versa.

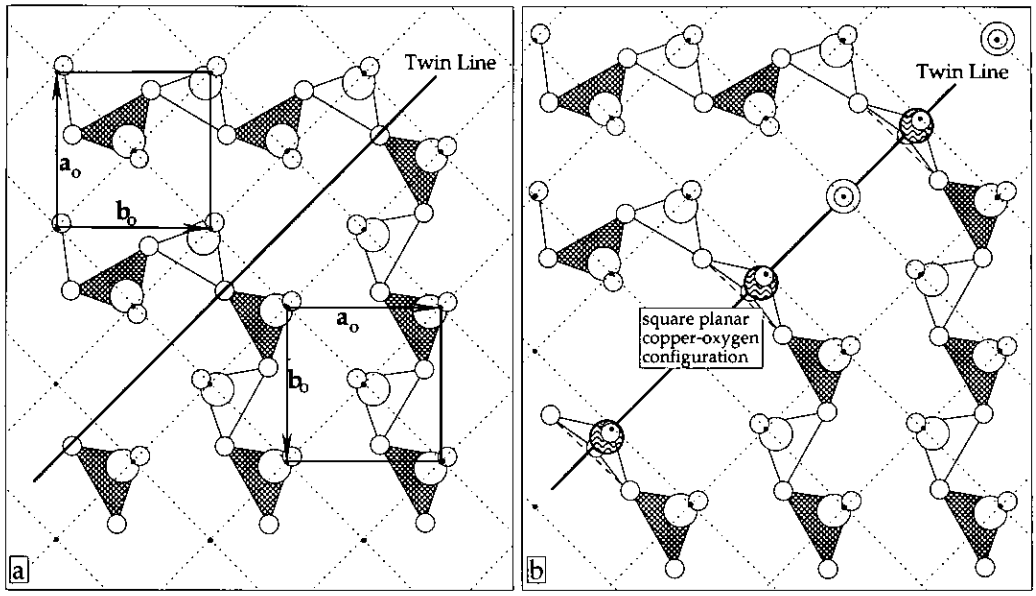

FIG. 4. Schematic representation of a twin line in the *M*O-layer of the substituted 123-intergrowth structure. (a) The twin line coincides with a line of oxygen atoms; (b) the twin line is localized through the heavy atoms which may be copper atoms forming deformed square planar configurations. O atoms are indicated by small circles, *M* atoms by large circles, Cu atoms by waved-circles, and a small black dot shows the "perovskite" Cu-position.

produced in Fig. 5a and as insets in Figs. 6 and 7b. The intense spots are produced by the perovskite blocks, whereas the weak spots in zones $[001]_o$ (Fig. 5a) and $[2\bar{1}0]_o$ (Fig. 7b) are due to a superstructure. The indexes with subscript o refer to an orthorhombic unit cell with dimensions $a_o \times b_o \times c_o$ ($a_o = a_p\sqrt{2}$; $b_o = a_p\sqrt{2}$; $c_o = 2c_p$, with $a_p \approx 3.8$; $c_p \approx 11.4$Å) (*8*).

The $[2\bar{1}0]_o$ zone (Fig. 7b) exhibits rows of superstructure reflections parallel to the c^*-axis; it shows that the unit cell must have a c-parameter $c_o = 2c_p$. Alternating rows show slightly elongated reflections; they correspond to the superstructure spots in the $[001]_o$ zone.

The presence of the weak spots indicates that a superstructure is present with unit cell dimensions $a_s \times b_s \times c_s$ ($a_s = 2a_o$; $b_s = b_o$; $c_s = c_o$). From the different sections the reciprocal lattice was derived and is represented in Fig. 8a as viewed along the $[001]_o$ zone. The l-coordinates of the reciprocal lattice nodes are cited in the legend. The indexes with subscripts p, o, and s refer to the pseudotetragonal perovskite unit cell ($a_p \times b_p \times c_p$), the diagonal orthorhombic unit cell, and the superlattice unit cell, respectively.

Very often, the selected area contains two orientation variants, differing by a rotation over 90° about the c-axis. This can be deduced from the high resolution images to be discussed below. The resulting diffraction pattern then has apparently tetragonal symmetry along the $[001]_o$ zone (Fig. 9).

4.2. The n212-Ga-Compound

Sections of reciprocal space of the 2212-Ga-phase along the zones $[010]_o$, $[100]_o$, $[2\bar{1}0]_o$, and $[1\bar{1}0]_o$ are reproduced in Fig. 10. Except for the $[2\bar{1}0]_o$ zone these patterns are not very different from the homologous patterns produced by the 1212-Co-compound. The $[001]_o$ zone of the 2212-Ga-compound is compared with the $[001]_o$ zone of the 1212-Co-compound in Fig. 5. From these patterns the reciprocal lattice repre-

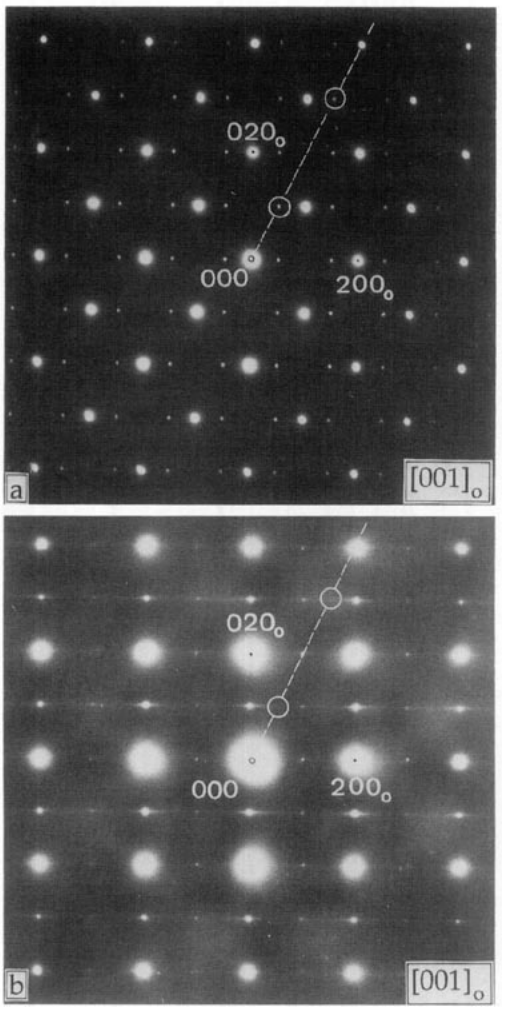

FIG. 5. Diffraction pattern of the two $n212$-intergrowth phases along the [001] zone: (a) Co-1212, (b) Ga-2212. The section through the streaks present in the $[210]_o$ zone (Figs. 10d and 7b) is indicated.

sented in Fig. 8b, as viewed along the $[001]_o$ zone, was constructed and indexed in the same way as described above, using the same symbols.

In the $[2\bar{1}0]_o$ zone pattern alternating rows parallel to c^* are continuously streaked; also the other spot rows are slightly streaked along the c^*-direction. The spots observed in the $[001]_o$ zone and which correspond to the intersections of the continuous streaks of the $[2\bar{1}0]_o$ zone pattern of Fig. 10d are very weak. They are encircled in Fig. 5.

The most striking difference consists in the absence in the $[001]_o$ zone of the strong spots at positions $(110)_o$, which, as we shall see, is a consequence of the presence of a double fluorite-like layer, causing a relative shift over $\frac{1}{2}$ $[110]_p$ of the two perovskite blocks.

The diffraction pattern taken along the $[1\bar{1}0]_o$ zone, from an area containing intergrowths of the two $n212$-Ga-phases ($n = 1$ and $n = 2$) with two different thicknesses of the fluorite-like lamellae, is reproduced in Fig. 11. Note that the two superimposed patterns have different geometrical features. The pattern corresponding to the smaller c-spacing ($c_1 = 2.28$ nm) has a rectangular mesh outlined by solid lines in Fig. 11, showing that the orthorhombic reciprocal unit cell is not body centered. This is consistent with the presence of a single rare-earth layer in the structure. The pattern corresponding to the larger c-spacing ($c_2 = 2.82$ nm) has a centered unit mesh outlined by dotted lines in the figure; it shows that this reciprocal unit cell is body centered, which is consistent with the presence of a double layer rare-earth oxide lamella, causing a relative shift of successive perovskite blocks.

Ignoring the weak reflections due to the superstructure, the diffraction conditions deduced from the reciprocal lattices of the 1212-Co- and the 1212-Ga-compounds are compatible with the space group $Ic2m$.

5. Structural Models

5.1. Preliminary Remarks

We shall first discuss an idealized structure model for the 1212-Co-compound since for this material well-defined diffraction patterns, largely free of diffuse scattering, are available for all relevant zones. Moreover the complications arising from the possibility of a relative shift of two successive perovskite blocks, which may also lead to faulting, are avoided.

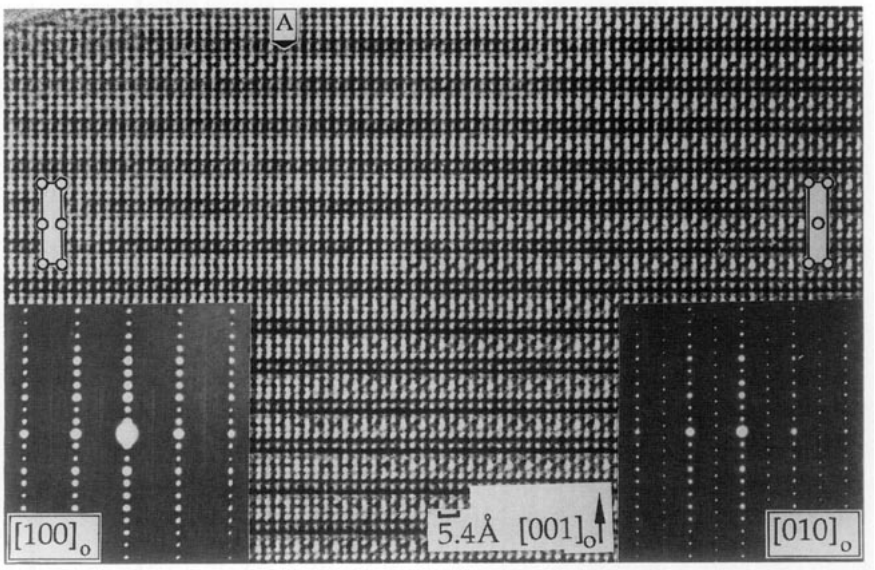

FIG. 6. High resolution image of an area of Co-1212-phase containing two orientation variants of the superstructure. In the left part the structure is viewed along the $[100]_s$ zone which is normal to the chain direction, whereas in the right part the chains are viewed along their length axis, i.e., along $[010]_s$. Note the staggered arrangement of the bright (or dark) dots situated in the CoO-layers.

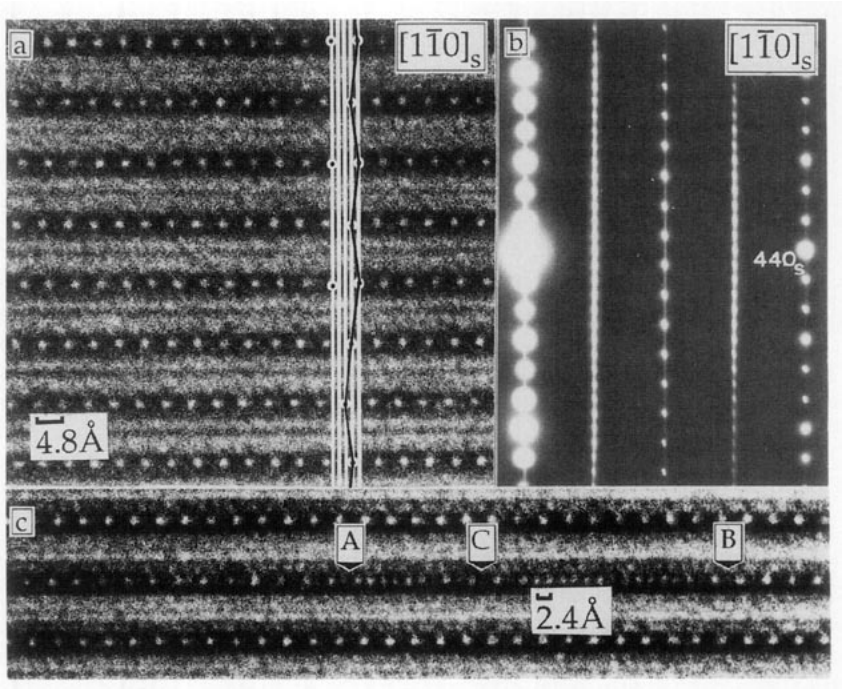

FIG. 7. High resolution image of the Co-1212-phase along the $[110]_s$ zone. Most atomic layers are imaged as lines, due to the small intercolumn separation. In the CoO-layers the bright dots reveal the superstructure (spacing, 0.48 nm). (a) The regular stacking can be observed in the upper five dot rows; in the next row a defect appears. (b) The corresponding diffraction pattern is shown. In certain CoO layers ((c), A to B) also the 0.24-nm spacing between bright dots is revealed, indicating the presence of an intralayer line defect. Note that the widely spaced dot arrays in A (or B) and in C are out of phase. The $[001]_s$ direction points upward.

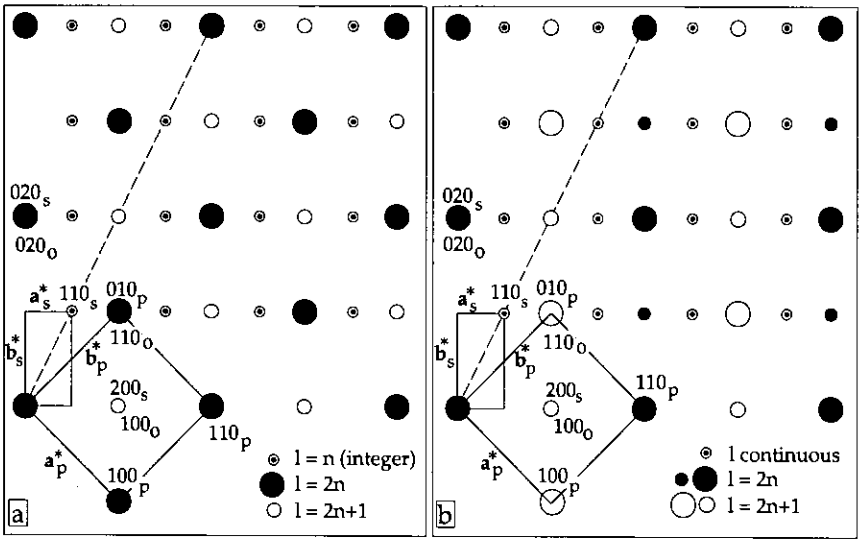

FIG. 8. Schematic representation of the reciprocal lattices as viewed along the [001] zone (a) for the 1212-Co-compound, and (b) for the 2212-Ga-compound. The unit meshes of the basic perovskite lattice (a_p^*, b_p^*) and of the superstructure (a_s^*, b_s^*) are indicated. Superstructure reflections are indicated by encircled black dots.

5.2. The 1212-Co-Compound

From the [001] zone diffraction pattern of Fig. 5a it is clear that the 110_o reflection is prominently present, which would suggest that the reciprocal lattice is face centered and hence that the lattice is body centered, as proposed in (*6*) and (*8*). The other basic sections of reciprocal space show that

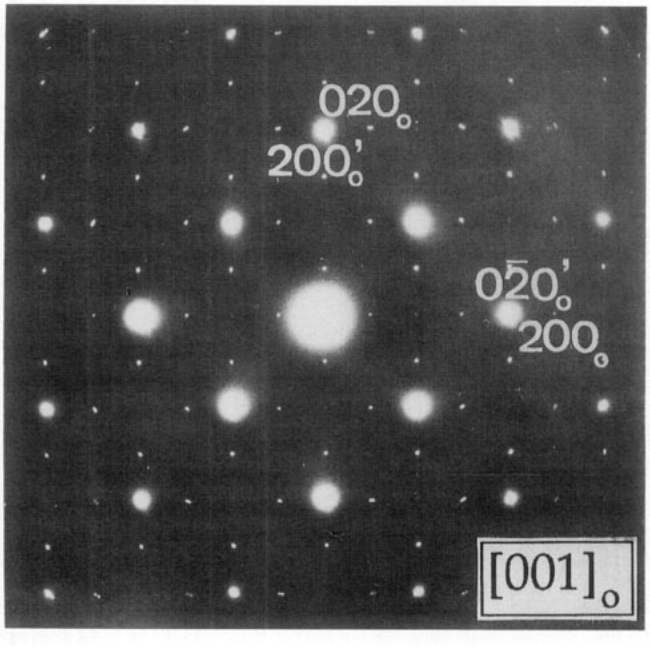

FIG. 9. Diffraction pattern along the $[001]_o$ zone of an area containing two orientation variants differing by a 90° rotation about the *c*-axis.

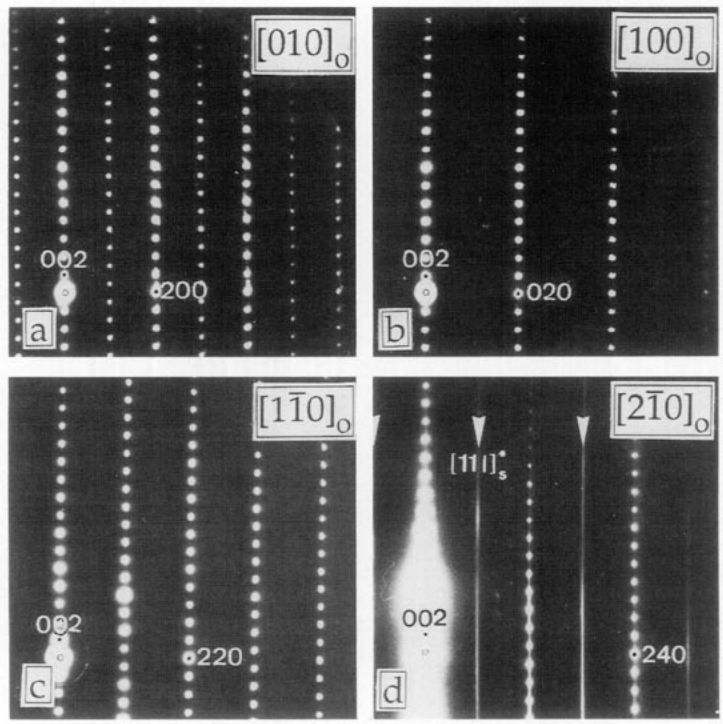

FIG. 10. Diffraction patterns of the 2212-Ga-intergrowth phase along different zones. (a) $[010]_o$ zone: The staggered arrangement of spots shows the B-centering of the chain lattice, (b) $[100]_o$ zone: Note the absence of centering along this zone; (c) $[1\bar{1}0]_o$ zone, (d) $[2\bar{1}0]_o$ zone. The continuous streaks marked by arrowheads are due to disorder in the superstructure.

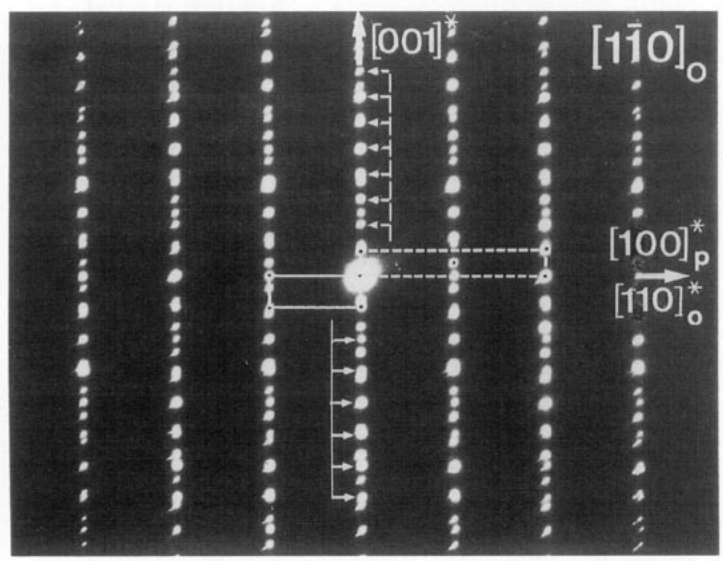

FIG. 11. Diffraction pattern of the *n*212-Ga-intergrowth structure along the $[1\bar{1}0]_o$ zone. The selected area contains two phases with different *c*-parameters: $c^{(1)} = 2.28$, $c^{(2)} = 2.82$ nm, corresponding with compounds containing respectively a single and a double fluorite-like lamella.

whereas the $[010]_o$ (or $[010]_s$) zone pattern is centered as well, this is not the case for the $[100]_o$ (or $[100]_s$) zone pattern (Fig. 6). The lattice based on the unit cell $\sqrt{2}a_p \times \sqrt{2}a_p \times 2c_p$ is nevertheless body centered, systematic extinctions preventing centering of the $[100]_o$ zone. This is consistent with the space group *Ic2m* found in (*6*) for the 1212-Ga-compound.

The presence of the $(110)_o$ reflections in the $[001]_o$ zone finds actually its origin in the fact that the arrangement of the perovskite blocks (ignoring the *M*O-chain layers) is C-face centered in the orthorhombic description, and thus leads to a centered unit mesh of intense reflections in the $[001]_o$ zone. On the other hand, the staggered chain sublattice is B_o-centered since we cannot distinguish L- and R-chains when viewing along the chain direction; therefore, the $[010]_o$ (or $[010]_s$) zone pattern also has a centered unit mesh $\sqrt{2}a_p \times 2c_p$. The discussed diffraction patterns are consistent with a model in which all chains are equal, but equally well with a model in which L- and R-chains parallel to b_o alternate along a_o since the projected structures are the same in successive *c*-layers for both models. The intense spots, which are due to the averaged structure of a single orientation variant, are thus accounted for.

Differentiation of the two models is possible by viewing along certain oblique sections or along the $[001]_o$ zone. It is clear that the body centered *Ic2m* space group found in (*6*) and (*8*) must be considered as referring to a structure averaged over the different variants. This is also suggested by the observation of the split positions of the oxygen atoms proposed in (*2*).

We have noted above the L- and R-chains are equally probable; they should therefore occur in equal numbers, either in separate crystal parts or within the same crystal. The doubling of the lattice parameter along a_o ($a_s = 2a_o$), as required by the weaker spots in the $[001]_s$ and $[1\bar{1}0]_s$ diffraction patterns, can be achieved in a natural way by assuming alternating parallel CoO-chains are different (but energetically equivalent). The logical assumption is therefore that L- and R-chains alternate in a given CoO-layer as shown in Fig. 12b.

Chains of the same type can be formed with respect to the underlying perovskite block in four different positions, related by displacement vectors $\frac{1}{4}[120]_s$, $\frac{1}{2}[100]_s$, and $\frac{1}{4}[\bar{1}20]_s$, as shown in Fig. 13. The positions (*a*) and (*b*) of course can not be occupied simultaneously in the same CoO-layer, since the same Co-atoms would be involved

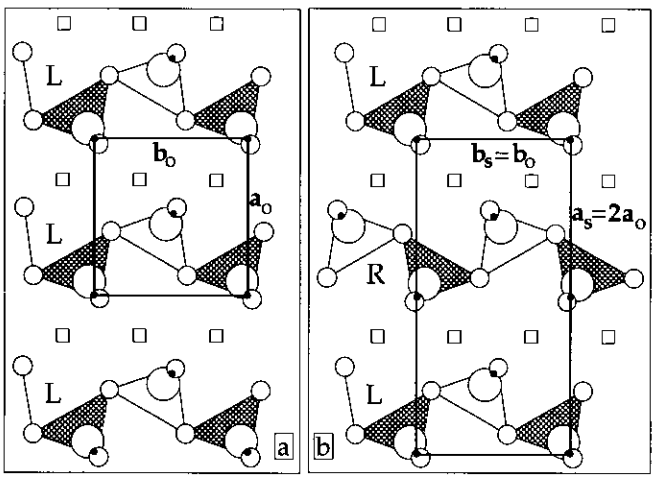

FIG. 12. Models for the structure of the chain layer *M*O. (a) All chains are of the same type, (b) L- and R-chains regularly alternate. The unit meshes are indicated by solid lines.

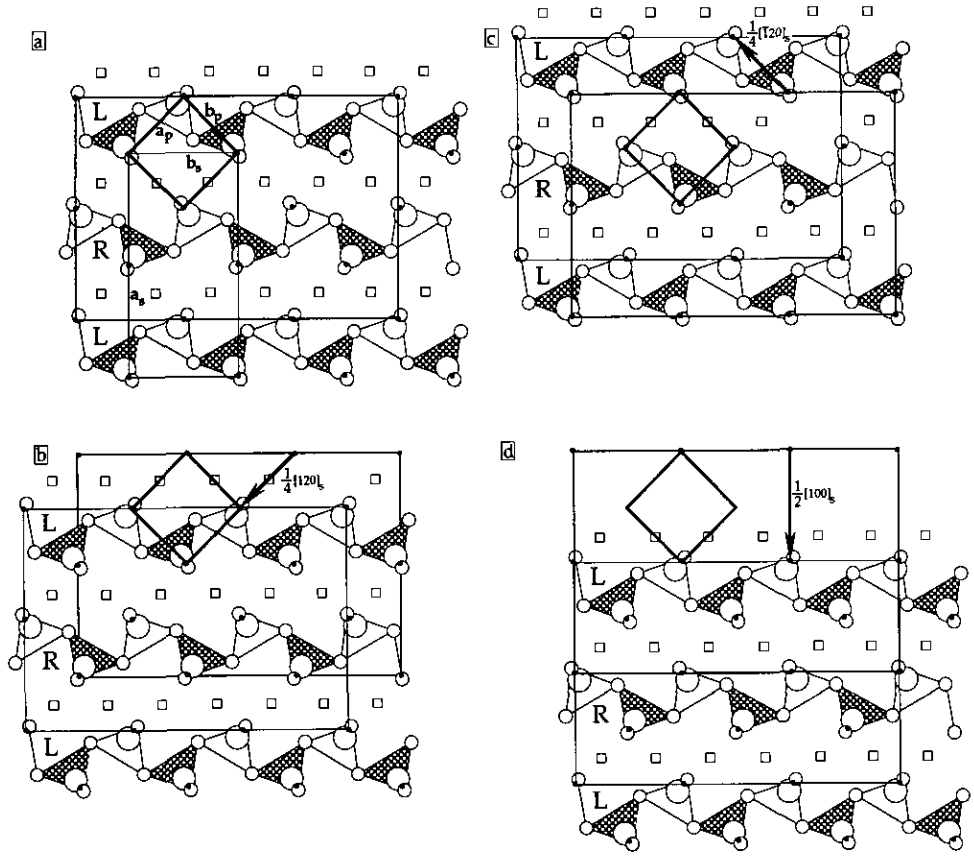

FIG. 13. The four possible arrangements of the *M*O-alternating chain layer, (a), (b), (c), and (d), with respect to the underlying perovskite block, indicated by small black dots. The rectangle and the perovskite unit cell in heavy lines serve as reference. The different positions are characterized by a displacement vector relative to the reference rectangle.

in two chains. However, it is plausible to assume that chain positions within the same layer differing by a translation $a_o = \frac{1}{2}a_s$, such as (*a*) and (*d*), can a priori be occupied either by chains of the same type as was assumed by Roth *et al.* (*6*) or alternatively by chains of opposite type as we propose here. From the occurrence of split oxygen positions in neutron diffraction, there is some indication that two types of chains may occur (*6*, *8*).

We note moreover that also the *c*-axis (c_s = 2.28 nm) must be doubled as compared to that of the reference 123-compound (c_p = 1.14 nm). Since the perovskite blocks are stacked vertically, this must be achieved by a staggered configuration of the chain positions in the successive CoO-layers, as required by the $[010]_o$ diffraction pattern of Fig. 6. The vertical stacking of chains can be excluded on this basis.

Doubling of the a_o and c_p parameters can be achieved simultaneously if the sublattice of chain positions has a B-centered unit cell and if moreover within each layer chains of different type alternate on this sublattice. We show that such a model for the superstructure is consistent with the observed diffraction patterns.

A characteristic feature of the $[001]_s$ diffraction pattern of Fig. 5a, produced by a single variant of the Co-superstructure, is that the superstructure reflections with h =

$4m + 2$ (m integer) for k even, as well as those with $h = 4m$ for k odd, are systematically absent. In the $[1\bar{1}0]_s$ section of Fig. 7 the rows with $h = k =$ odd contain superstructure spots for all l, whereas rows with $h = k = 4m + 2$ contain only spots for l odd. The rows with $h = k = 4m$ coincide with the spots due to the basic structure. Extinctions can of course only be observed where such superstructure reflections do not coincide with rows of reflections due to the basic perovskite structure.

In the Appendix, it is shown that all these observations can be explained consistently by assuming a perfect . . .–L–R–L–R– . . . arrangement of parallel chains, $a_o = \frac{1}{2}a_s$ apart, in the CoO-layers, the arrangements in successive CoO-layers being related by a translation $\frac{1}{4}[122]_s$, as shown in Fig. 13. The systematic extinctions of the superstructure reflections due to the CoO-chains are fully accounted for on the basis of this model (see Appendix).

To derive the space group, the diffraction conditions cannot be used as such, since they are more restrictive than those associated with any one of the 230 space groups. However, following a reverse reasoning, a space group can be deduced from the proposed model. The two-dimensional group of the proposed chain arrangement in the CoO-layer is $P2gg$. The space group resulting from the spatial arrangement of these layers, i.e., of the CoO-sublattice, is $Pca2_1$ (No. 29). It is a subgroup of the $Ic2m$ space group of the structure in which all chains are assumed to be identical (*6*). With this space group being itself closely related to subgroups of the space groups $Pmmm$ and $P4/mmm$ of $YBa_2Cu_3O_7$ and $YBa_2Cu_3O_6$, respectively, it can be concluded that the space group of the CoO-sublattice is in turn a subgroup of that of the perovskite block. We can therefore conclude that $Pca2_1$ has to be the space group of the complete structure, since it is only the chain structure which reduces the symmetry of the 123-structure. The more restrictive diffraction conditions are to be attributed to the special positions associated with the specific arrangement of the chains, as discussed in detail in the Appendix.

5.3. The 2212-Ga-Compound

The differences between the $[001]_o$ diffraction patterns of the 1212- and 2212-phases are mainly due to the larger degree of disorder in Fig. 5b as compared to Fig. 5a, but the absence of strong (basic) spots at the 110_o position in Fig. 5b is the most striking feature. It is due to the presence of the relative shift over $\frac{1}{2}[110]_p$ between the successive perovskite blocks in the 2212-Ga-compound, which causes body centering of the basic "perovskite" unit cell or face centering of the $\sqrt{2}a_p \times \sqrt{2}a_p \times c_2$ unit cell, as opposed to the C-centering of the $a_o \times b_o \times c_1$ cell in the 1212-compound. In the orthorhombic description this leads to face centering of the unit cell and hence to the body centering of the corresponding reciprocal lattice. This is in agreement with the $[110]_o$ section shown in Fig. 10c for the 2212-compound and in Fig. 11 for overlapping $[1\bar{1}0]_o$ sections of both 1212- and 2212-compounds. The $[010]_o$ zone (Fig. 10a) is centered as a result of the chain arrangement and not because of the arrangement of the perovskite block.

The streaks along c_s^* in Fig. 10d and along a_s^* in Fig. 5a can be attributed to the presence in reciprocal space of ribbon shaped regions of diffuse scattering with their length axis parallel to c_s^* and extending in width along the a_s^* direction. The observed streaks are the intersections of Ewald's sphere with such ribbons. The shape of these diffuse intensity regions suggests that two different types of disorder occur simultaneously: pronounced one-dimensional disorder of layers along c_s and less pronounced disorder of chains within the layers, along a_s.

The disorder along a_s can be attributed to the violation of the alternating L–R arrangement of parallel chains. The high resolution images suggest that the site lattice of the chains is rather perfect (Fig. 14). Conse-

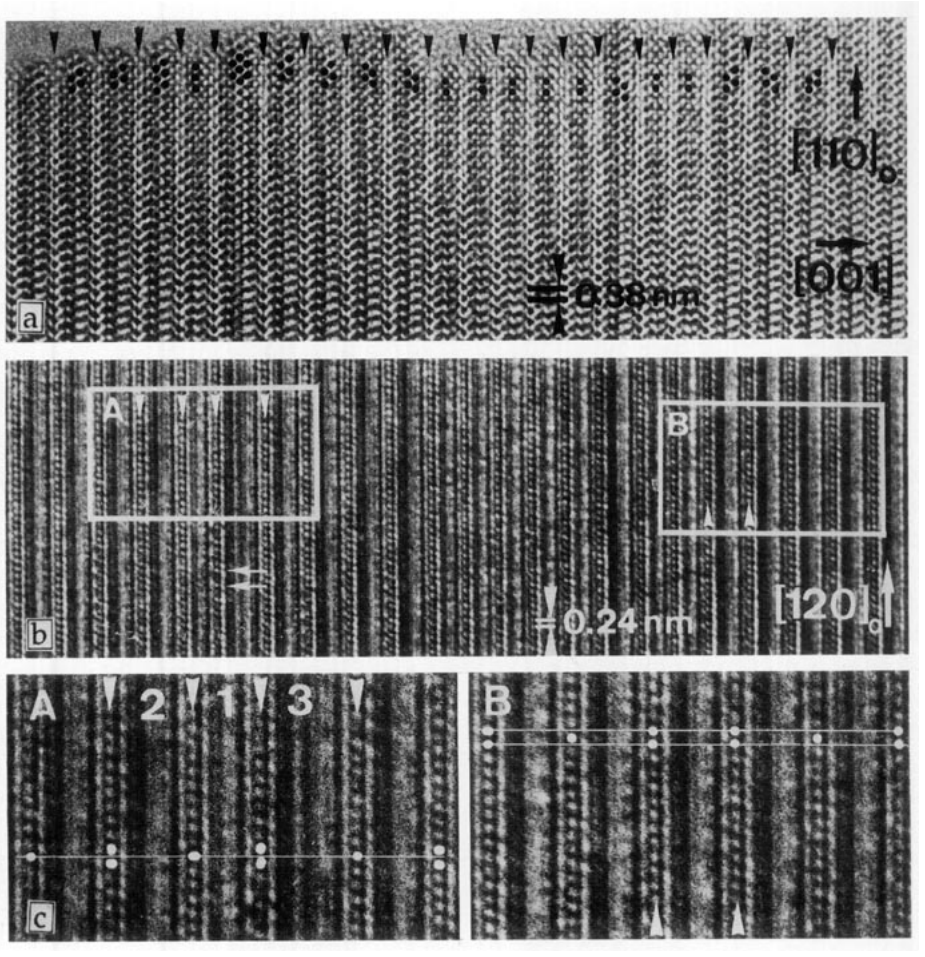

FIG. 14. High resolution image of $n212$-Ga-compound: (a) along the $[1\bar{1}0]_o$ zone. Note the presence of rare-earth oxide lamellae of different thicknesses: one, or three layers. The rare-earth columns have been marked by dots. (b) The same area as in (a) imaged along the $[1\bar{2}0]_o$ zone. Except for the GaO-layers, which are imaged as dots (c), all other layers are imaged as lines. Two areas A and B are magnified in the insets. The staggered arrangement of the bright dots irrespective of the number of rare-earth layers in fluorite-like lamellae is emphasized in A. Exceptionally, two vertically stacked layers are present in B.

quently, the disorder must be attributed to the occupation of this sublattice by L- and R-chains, i.e., to deviations from the regular alternations of R- and L-chains. Such disorder leads to Lorentzian broadening (*21*) along a_s^* of all superlattice reflections since it effectively leads to a distribution of projected spacings of $a_o, 2a_o, 3a_o, \ldots$, centered around $2a_o$, between chains of the same kind. This is apparently more pronounced in the Ga-compounds than in the Co-compound, as can be judged from Figs. 5a and 5b. When such disorder within the layers is present, inevitably stacking disorder must also be present along c, leading to streaks along c_s^*. The reverse is *not* true however. Perfectly L–R ordered parallel chain layers may still be stacked along c in a disordered way, and give rise to streaks along c_s^* without broadening along a_s^*. Not all reflections become streaked however. If $\mathbf{R}$ is the vector connecting the correct stacking position with the faulted one, only reflections $\mathbf{g}$ for which $\mathbf{g} \cdot \mathbf{R} \neq$ integer will

be streaked (*22*). In the present case the displacement vector leads from the position $\frac{1}{4}$ $[102]_s$ to $\frac{1}{4}$ $[\bar{1}02]_s$ and is thus $\frac{1}{2}$ $[100]_s$, and hence, only superstructure reflections with

$$h_s = \text{odd} \qquad (1)$$

will become streaked along c^*.

Allowing also for the fact that occasionally a vertical stacking of the chain arrangement occurs instead of the normal staggered stacking (Fig. 14c B), faults with a displacement vector, leading from the position $\frac{1}{2}$ $[011]_s$ to $\frac{1}{4}$ $[102]_s$, i.e., $\frac{1}{4}$ $[120]_s$, should be considered as well. Applying the same reasoning as above, they lead to streaking of the superstructure reflections for which

$$(h + 2k)_s \neq 4\text{-fold}. \qquad (2)$$

The conditions (1) and (2) account satisfactorily for the presence of the diffuse streaks in Figs. 10d and 5b.

The presence in certain specimen areas of a mixture of single and double fluorite-like lamellae is a further source of diffuse streaking along c_s^*. The fault vector is in this case $\frac{1}{2}$ $[110]_p$; it therefore causes streaking of the basic reflections with $(h + k)_p$ = odd. A disordered mixture of single and double fluorite-like lamellae will also lead to streaking of the fundamental reflections along the c^* direction.

Finally, the presence of superposed lamellae belonging to different 90° orientation variants would cause further complications in the diffraction pattern. Along the [001] zone the diffraction pattern could acquire fourfold symmetry due to the superposition of two diffraction patterns such as Fig. 5, differing 90° in orientation (Fig. 9).

6. High Resolution Imaging

6.1. The Basic Structure

6.1.1. The 1212-Co-compound. High resolution images of sufficiently thin parts of the specimen reveal directly the different layers of the structure. Only the basic structure is revealed when imaging along those zones which correspond to reciprocal lattice sections in which no extra superlattice spots are present. These zones include the $[100]_o$, $[010]_o$, $[110]_o$, and $[1\bar{1}0]_o$. In Fig. 6 the $[010]_o$ zone image (on the right side) as well as a $[100]_o$ zone image (on the left side) is reproduced with the corresponding diffraction patterns. Assuming all cobalt to substitute for copper in the CuO-layers of the reference structure, the layer sequence is

$$\ldots\text{–SrO–}CuO_2\text{–}$$
$$\text{Y–}CuO_2\text{–SrO–CoO–}\ldots$$

The CoO-layer can be identified from symmetry considerations, as it is clear that it must be located on a (001) mirror plane for the structure. Two such mirror planes are present, the other being the Y-layer. Since the Y-layer is imaged identically along $[010]_o$ and along $[100]_o$, the CoO-layers can be identified; they are indicated in Fig. 6 by small circles, marking unit cell node points. This layer being located, the other layers can easily be labeled. Since the CoO-chains of corner-linked tetrahedra are parallel to $[010]_o$, the $[010]_o$ zone images are of particular interest. Along this direction, the CoO-chains are imaged as rows of bar-shaped dots separated by 0.54 nm. Irrespective of whether the cobalt columns are imaged as bright or dark dots, the image proves that they occur in a staggered arrangement viewed along $[010]_o$. In this case the staggering cannot be attributed to a relative shift of the perovskite blocks since only a single rare-earth layer is present.

Anticipating the discussion of the superstructure, it is worth noting that along this zone L- and R-chains produce the same contrast since their projection along the viewing direction is the same. This image thus reflects an averaged structure, consistent with the structure proposed in (*6*, *8*).

6.1.2. The n212-Ga-compounds. Figure 15 shows an image of the $n = 2$ compound as viewed along the $[110]_o$ zone. The different layers can again be identified from symmetry considerations similar to those in the previous paragraph. It is evident from the

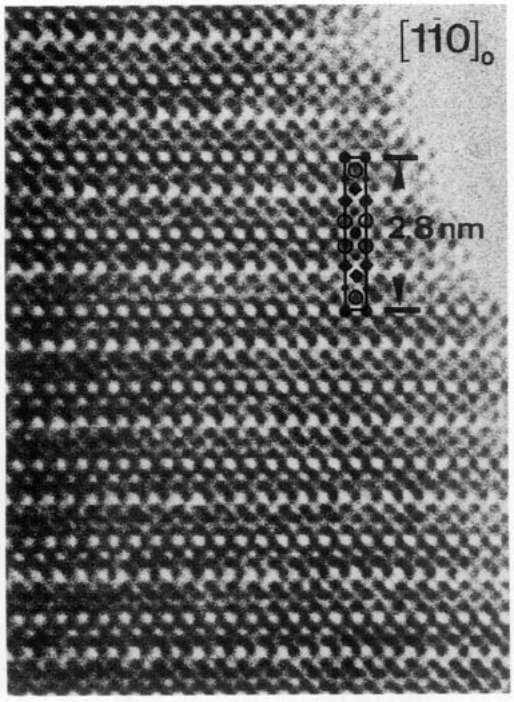

FIG. 15. High resolution image of the 2212-Ga-compound along the [1$\bar{1}$0]$_o$ zone. The atom columns are imaged as dark dots. The open dots represent strontium columns, and the squares represent the rare-earth columns in the fluorite-like lamella. The large full dots represent Ga atom columns, and the small full dots represent copper atoms in the CuO_2-layers. Oxygen atoms are not imaged.

known layer sequence (*13*)

. . .–GaO–SrO–CuO_2–
(Nd/Ce)O_2(Nd/Ce)–CuO_2–SrO–. . .

that the only monoatomic layer which occurs only once in the repeat unit and which is moreover located midway between two multilayered lamellae which are mirror images with respect to that layer must be the GaO-layer. Once this layer is recognized, the other layers can easily be identified (Figs. 14 and 15). The interpretation must also be consistent with the occurrence of fluorite-like layers of different thicknesses; i.e., the dot rows assimilated with the fluorite-like lamellae must be the only ones that differ in multiplicity (1, 2, 3, . . .) in the three members of the homologous series (Fig. 14a). Also the lateral shift, when present, i.e., when the number of layers is even, between successive perovskite blocks occurs at the fluorite-like layers. These considerations have led to the image interpretation shown in Fig. 15, where black squares indicate the fluorite-layers.

6.2. The Superstructures

6.2.1. The 1212-Co compound. The $[010]_o$ image of Fig. 6 has proved that the CoO-chains in successive layers adopt a staggered arrangement, their separation within the layer plane being 0.54 nm. Information on the superstructure can only be obtained from reciprocal lattice sections involving rows of superlattice reflections such as the $(1\bar{1}0)_s^* = (210)_o^*$ section shown in Fig. 7b. Apart from the $[22l]_s^*$ and the $[44l]_s^*$ rows, produced by the basic $\sqrt{2}a_p \times \sqrt{2}a_p \times 2c_p$ lattice, this section contains rows of sharp reflections $[11l]_s^*$ and $[33l]_s^*$ which are exclusively produced by the superstructure. The lattice spacing corresponding to the $[44l]_s^*$ perovskite reflections is too small ($\cong$0.12 nm) to be resolved in this section; with the 220_s reflection in the first row of sharp spots $[22l]_s^*$ corresponds a spacing of 0.24 nm. The spacing corresponding to the first superstructure reflection 110_s is 0.48 nm; spacings of 0.24 and 0.48 nm can be resolved.

The image of Fig. 7a along the $(1\bar{1}0)_s^*$ zone axis, corresponding to the diffraction pattern of Fig. 7b, shows bright dot rows with a spacing of 0.48 nm which must be attributed to the superstructure (no such spacing is present in the basic structure). In the major part of the area the bright dot sequences in successive rows are shifted over one-quarter of the interspot distance alternatively to the left and to the right. This zigzag arrangement of the dots viewed along this zone axis is related to a staggered arrangement of the chains. The observation supports the model proposed above for the stacking of successive *M*O-layers. Successive layers are zigzag-stacked, related by vectors $\frac{1}{4}[122]_s$ and $\frac{1}{4}[\bar{1}22]_s$, as shown sche-

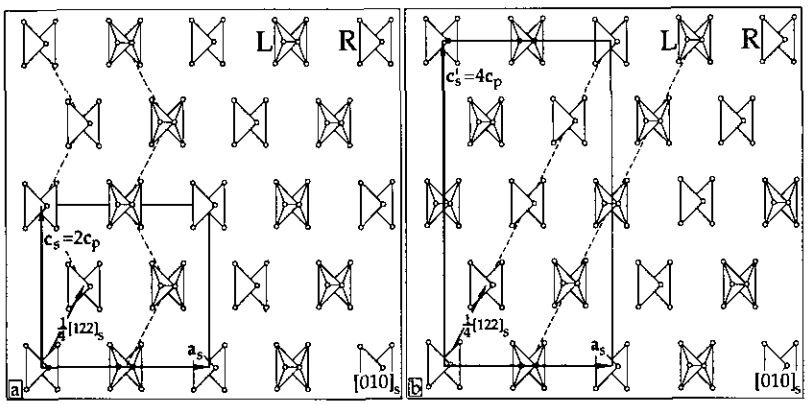

FIG. 16. Arrangement of chains as viewed along the $[010]_o$ direction: (a) Staggered arrangement. The vector connecting two similar chains in successive layers is indicated. The repeat period is $c_s = 2c_p$. The stacking can be described as . . .–*a*–*b*–*a*–*b*–*a*–*b*–. . . using the notation introduced in Fig. 8. (b) Oblique arrangement leading to a repeat period of $4c_p$. This stacking can be represented by the symbol sequences . . .–*a*–*b*–*c*–*d*–*a*–*b*–. . . . Bright dot arrangements, which image these stackings, are observed in Fig. 7.

matically in Fig. 16a. Occasionally the one-quarter shift proceeds two or three times in the same sense; locally the layers are then stacked as in Fig. 16b with a cumulative translation from layer to layer with the same vector $\frac{1}{4}[122]_s$.

In Fig. 7a the CoO-chains are viewed along the $[110]_s$ direction under an oblique angle as represented schematically in Fig. 17 where the arrows are parallel to the viewing direction. Assuming all chains to be equivalent (either all L or all R) as in Fig. 17c, the heavy Co atoms are situated on zigzag columns, which are all equivalent

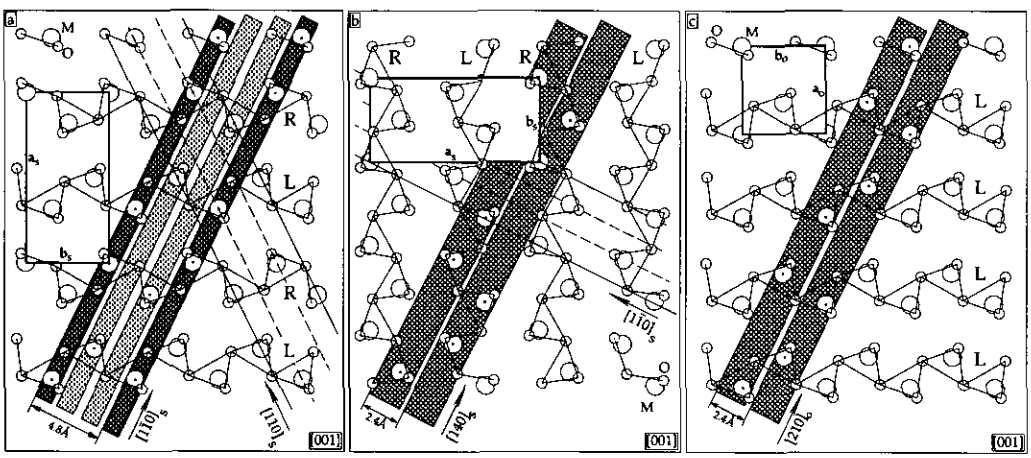

FIG. 17. (a) Schematic representation of a layer of *M*O containing an alternation of L- and R-chains. The largest circles represent *M* atoms, the smaller ones O atoms. Identical columns along the $[110]_s$ viewing direction are indicated by identical shaded bands; the presence of two different types of columns leads in the image to a period of 0.48 nm. (b) When viewed along the $[140]_s$ zone all columns produce equivalent images, leading to a period 0.24 nm. (c) If all chains are of the same type all columns in the $[110]_s$ view are equivalent, the period being 0.24 nm.

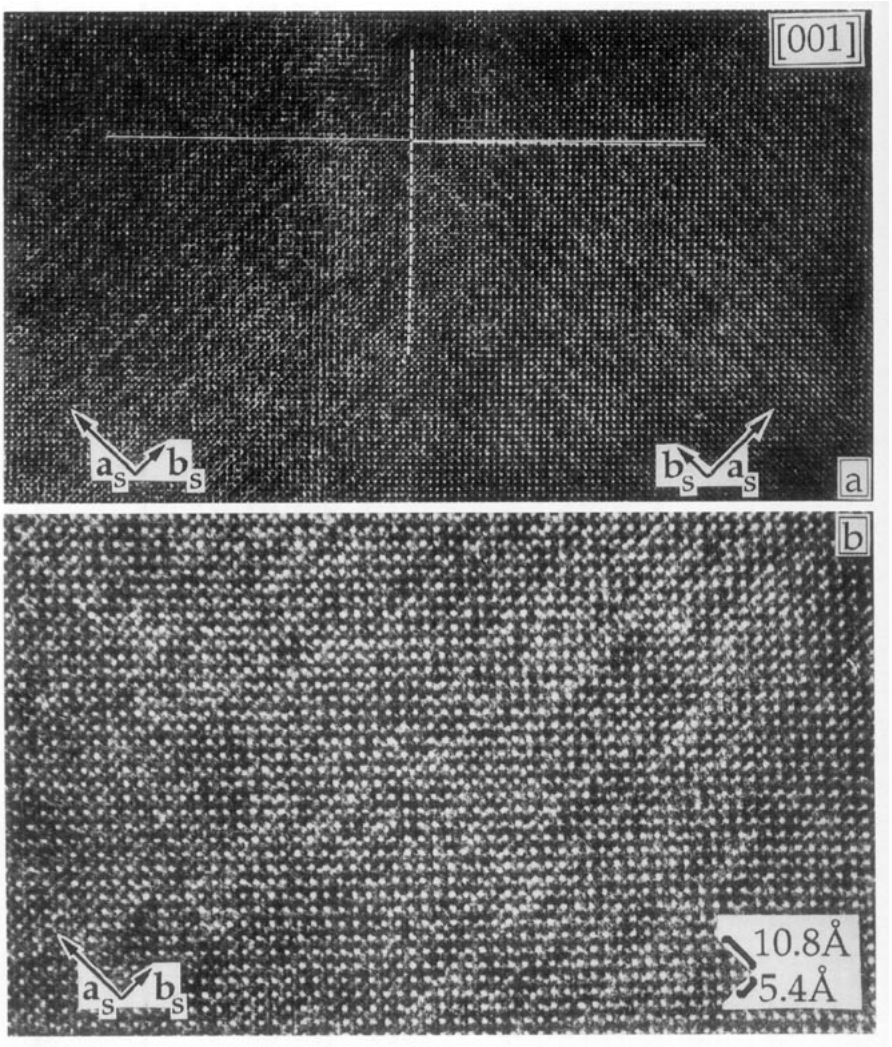

FIG. 18. High resolution image along the [001] zone of the 1212-Co-compound: (a) low magnification: note the presence of brightness modulations along $[110]_p$ and $[1\bar{1}0]_p$ showing that a vertical twin boundary is present. The horizontal dot rows suffer a small orientation change across the twin boundary; this proves that a_o and b_o are slightly different in length; (b) high magnification of a small area of (a), showing that the modulation period is two orthorhombic cells wide, i.e., $a_s = 2a_o = 2a_p\sqrt{2}$.

and which have a spacing of 0.24 nm. Also the "channels" of oxygen atoms between the Co-columns are all equivalent and have the same spacing 0.24 nm. In the case of an alternation of L- and R-chains in the CoO-layer, Fig. 17 demonstrates that in images along $[110]_s$ and $[140]_s$ two types of dot rows can occur, one with a spacing of 0.48 nm (Fig. 17a) and one with a spacing of 0.24 nm (Fig. 17b), depending on the orientation of the CoO-chains. As suggested above, stacking of the chain layers imaged as the dot rows in Fig. 7 must thus be attributed to the alternation of the L- and R-chains in the chain array represented schematically in Fig. 16a.

The image of Fig. 18 taken along the [001] zone exhibits a weak modulation along the two $[110]_p$ and $[1\bar{1}0]_p$ directions, the period being 1.1 nm, i.e., $\approx 2 \times 0.54$

nm, in accordance with the proposed model for the superstructure.

6.2.2. The n212-Ga-compound. For the *n*212-Ga-compound the high degree of disorder in the L–R-stacking of the chains in the Ga-O-plane was already revealed by the presence of streaky segments in the $[001]_s$ diffraction pattern (Fig. 5a), as compared to the sharp superstructure spots in the 1212-Co-case (Fig. 5b) for 2212-Ga. In the image of Fig. 14b, the heavy Ga atoms are situated in zigzag columns in the GaO-plane, with the average spacing of 0.24 nm; they form a staggered array along the *c*-direction, irrespective of the number ($n = 1, 2, 3$) of layers in a fluorite-lamella (Fig. 14c A). Only exceptionally a vertical stacking (Fig. 14c B) appears in a slab of the 2212-Ga-compound (*23*). Nevertheless, the disorder in the arrangement of L- and R-chains on the chain sublattice is apparently so large that no superstructure is revealed. In the next section, we discuss the various defects that cause the high degree of disorder that conceals the superstructure in this compound.

The larger separation between successive GaO-layers in the *n*212-Ga-compound, compared to that between CoO-layers in the I212-Co-compound, possibly explains the different behavior of these compounds. To what extent the details of the preparation methods of the compounds play a role has not been investigated.

6.3. Defects

6.3.1. Orientational domain structure. Due to the two possible orientations of the *M*O-chains with respect to the perovskite structure a microstructure consisting of domains differing 90° in orientation is to be expected. Since the two chain directions are $[110]_p$ (and $[1\bar{1}0]_p$), the coherent twin interfaces would be in $(100)_p$ or $(010)_p$ planes. It is also possible that the $(001)_p$ acts as a contact interface. (The latter plane was favored for the related twins in $YBa_2Cu_4O_8$ where the $(CuO)_2$ double chains can have also two mutually perpendicular orientations (*24*)). The presence of such a domain structure is revealed in a diffraction pattern along the $[100]_o$ (or $[010]_o$) zone, taken over an area containing both variants. The higher order $h0l$ (or $0kl$) reflections appear split along the direction normal to c_o^* since a_o and b_o differ by about 2%. High resolution images along such a zone show the structure in two different orientations when such a boundary is present; this is the case in Fig. 6. In the left area the structure is viewed perpendicular to the chains (i.e., along $[100]_o$) whereas in the right hand area, it is viewed along the chains (i.e., along $[010]_o$). The transition between the two regions occurs gradually and it visibly extends over four to five unit cells. It does not occur along a well-defined interface, but the changeover points in successive layers tend to be aligned, leading to two domains in the figure. Near to the specimen edge a few isolated layers also exhibit a changeover (pointer A in Fig. 6). In such cases the domain size is smaller, as observed above, and very often the individual layers behave in a way which is noncorrelated with the neighboring layers. Such small misoriented domains, present as defects, lead to the streak observed in the diffraction pattern along the $[100]_o$ zone.

If Fig. 18 these domains have been imaged along the [001] zone. The weak brightness modulation of the dots differs 90° in orientation in the areas on each side of the vertical twin boundary. The small orientation difference between the lattice rows in the two components of the twin is indicated.

6.3.2. Antiphase boundary-lines and 90° twin-lines. In the thinnest parts of the specimen in the $[1\bar{1}0]_s$ view one observes in certain CoO-layers the presence of two types of dot sequences. Though most bright dot sequences have a spacing of 0.48 nm, a gradual transformation into sequences having an interdot separation of 0.24 nm has been observed in some areas (Fig. 7c, pointers).

This phenomenon can be explained by

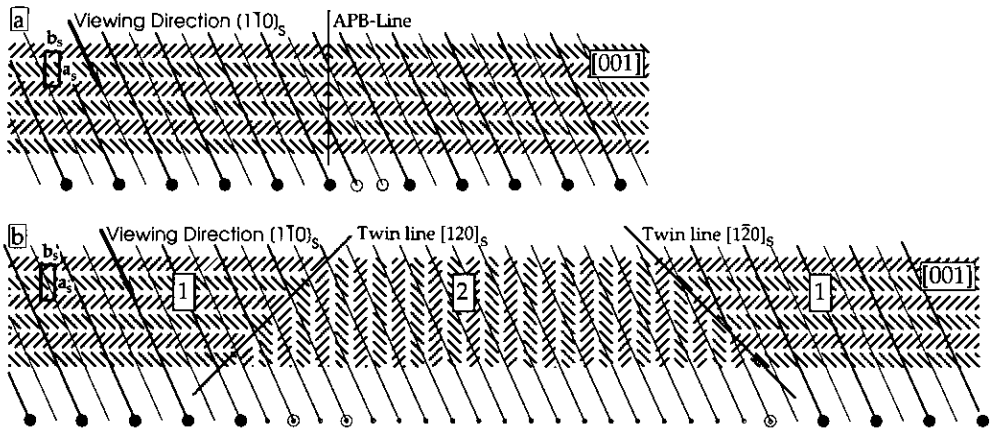

FIG. 19. Schematic representation of the image formation: (a) at an APB-line; (b) along two twin lines. The two kinds of chains are represented as bands, cross-hatched along two different directions. The full dots represent schematically the bright dots in the observed images, as viewed along the indicated direction.

assuming that within the same *M*O-layer the chains may change 90° in orientation, induced by various point defects, as discussed above in Section 2. This results in an effective change of the viewing direction by 90° with respect to the chain configuration, going from the $[1\bar{1}0]_s$ view, imaging the 0.48-nm spacing (schematically represented in Fig. 17a), to the $[140]_s$ view, imaging the 0.24-nm spacing (Fig. 17b). In Fig. 7c it is clear that along this new viewing direction, columns of CoO with a spacing of 9.24 nm are present. Either these columns or the channels between them are imaged. The occurrence of this feature is consistent with the small size of the orientation domains in the cobalt compound.

Within the same layer of CoO the phase of the 0.48 nm dot sequences may change occasionally by π (at pointer C in Fig. 7c); this always occurs through the insertion of a short sequence of dots with a 0.24 nm spacing (Figs. 19a and 19b).

This feature can be attributed to the presence of an "antiphase" boundary-line in the arrangement of the chains within the same layer of CoO. Along such an antiphase boundary-line, an L-chain becomes an R-chain, and vice versa. This is represented schematically in Fig. 9a, in a view along [001] where the different types of chains are represented by different hatching. The chains in one part of the layer are displaced with respect to those in the other part by a vector **R**. This clearly leads to a similar relative displacement of the atom columns in the two parts of the layer and hence, to a similar relative displacement of the dot patterns. This displacement thus finally leads to an interchange of the relative dot intensities in a sequence, i.e., to the observed change in phase of π. The APB is assumed to be situated in a $(010)_s$ plane, but this is not essential. The viewing direction is indicated and the two kinds of columns parallel to this direction are represented by heavy and light lines. The heavy lines represent those columns which are imaged as an intense bright dot, while the light ones are not imaged. Columns crossing the interface and thus consisting partly of segments of one type and partly of the other type are imaged by dots of an intermediate brightness. It is clear from Fig. 19 how the phase change over π comes about gradually. These observations suggest strongly the existence of antiphase boundary lines.

In most cases one observes a short segment of closely spaced weaker dots (0.24 nm spacing) inserted between two se-

quences of doubly spaced bright dots, which are "in phase." These observations can also be explained by the occurrence of small domains of orientation variants, i.e., 90° twins. In Fig. 19b the separating lines between the 90° microdomains are assumed to be coherent, i.e., to be along the $[110]_o$ direction; this is not essential however. The viewing directions are indicated; in domain 1 this is along $[110]_s$, and in domain 2 it is along a $[140]_o$ direction (Figs. 17a and 17b). In domain 2 all chains are imaged in the same way with the dot intensity being intermediate. In the case represented in Fig. 19b the bright dot sequences in both parts of domain 1 remain in phase, but depending on the exact positions of the boundary-lines these two parts may also be out of phase by π.

For an APB-line the width of the transition region is determined by the projected width of this line; for a microtwinned region the transition region may be much larger.

7. Discussion and Conclusions

The most important aspect of this work is the finding that the structures of the studied compounds differ from those published in the literature by the occurrence of a superstructure. The superstructure leads to a variety of order defects, well known in other systems, antiphase boundaries, and 90° twins, but also to some defects specific for the present structures and which could be termed antiphase boundary lines and 90° twin lines, since they are confined to one layer of either GaO or CoO.

High resolution images allow the localization of the layers responsible for the superperiod. Whereas a view along the chain direction $[010]_s$ (e.g., Fig. 6) reveals directly the chain stacking as an undistorted array, but does not discriminate between L- and R-chain orientations and thus only reveals an averaged stacking with 0.54-nm spacing between the chains, an image taken along the $(1\bar{1}0)^*_s$ section in which the superstructure spots are excited provides direct evidence that the superperiod is a consequence of ordering in the *M*O-layers; only the dot rows which image the *M*O-layers exhibit period doubling (Fig. 7).

A view long the $(1\bar{1}0)^*_s$ section (Fig. 7) indirectly reveals the stacking sequence, the relation between the actual configuration and the dot pattern being represented in Fig. 17. The dot configuration reflects the stacking of the chains only indirectly and in a distorted manner, but it does allow discrimination between a stacking consisting of all identical chains and a stacking consisting of L- and R-chains. If a periodic dot row associated with the *M*O-layer is assumed to be rigidly fixed in space with respect to the stacking of the chains, a relative shift of the *M*-layers over **R** will result in a relative shift of the two dot rows, which image these layers, over a vector which is the component of **R** normal to the viewing direction. This will be true even if the bright dots are not the images of single chains viewed along their axis, which is the case in Fig. 7. This figure thus proves that only a staggered arrangement of two types of chains will produce the observed image.

The model involving an alternation of two types of chains (Fig. 12b) implies almost inevitably the occurrence of stacking disorder since several stackings are possible (*23*) for which the energy difference only depends on the configuration of the second nearest neighboring *M*O-layers. Since the separation distance between such layers is large (1.14, 1.41, 1.68 nm, . . .), the interaction is weak and the energy difference very small. The "stacking information" is presumably transmitted mainly as a result of relaxation of the adjacent atom layers, possibly resulting in tilts of the CuO_5-pyramids (*6*), finally slightly favoring one type of chain over the other at a given site (*23*).

The different stacking possibilities for three successive layers are observed and represented schematically in Fig. 7, as observed through the $(1\bar{1}0)^*_s$ dot pattern. Some of the stackings, when repeated peri-

odically, would lead to repeat periods larger than $2c_p$. Such large repeat distances have not been observed in the diffraction patterns, but they occur locally as stacking faults in the 1212-Co-compound, leading to some weak streaking in the $[11l]_s^*$ and $[33l]_s^*$ rows of reflections (Fig. 7). In the 2212-Ga-compound, the disorder is more pronounced. The $(1\bar{1}0)_s^*$ image reveals the highly disordered stacking and there are no discrete spots in the superstructure rows of the diffraction pattern (Fig. 10d).

Appendix

We shall call F_o the structure factor of a CoO-layer containing one period of a regular succession of parallel –L–R–L–R– chains; F_o still depends on hkl. The chain configurations in the two CoO-layers in the unit cell of the superstructure are related by the translation $\frac{1}{4}[122]_s$ which is a symmetry translation of the perovskite blocks. The structure factor for the spatial superstructure of chains is then

$$F_{hkl} = F_o\{1 + \exp[(2i\pi/4)(h + 2k + 2l)]\}. \quad (1)$$

For $k + l$ = even, (1) reduces to

$$F_{hkl} = F_o[1 + \exp(i\pi h/2)]. \quad (2)$$

For

(a) h = 4-fold: $F_{hkl} = 2F_o$, $I_{hkl} \propto 4F_o^2$

(b) h = 4-fold ± 1: $F_{hkl} = F_o(1 \pm i)$, $I_{hkl} \propto 2F_o^2$ (3)

(c) h = 4-fold + 2: $F_{hkl} = 0$, $I_{hkl} = 0$.

For $k + l$ = odd, (1) reduces to

$$F_{hkl} = F_o[1 - \exp(i\pi h/2)]. \quad (4)$$

For

(a) h = 4-fold: $F_{hkl} = 0$, $I_{hkl} = 0$

(b) h = 4-fold ± 1: $F_{hkl} = F_o(1 \mp i)$, $I_{hkl} \propto 2F_o^2$ (5)

(c) h = 4-fold + 2: $F_{hkl} = 2F_o$, $I_{hkl} \propto 4F_o^2$.

It is evident that the extinction conditions deduced from (3) and (5) can be summarized as follows; reflections are absent if

$k + l$ = even, with h = 4-fold + 2;
$k + l$ = odd, with h = 4-fold.

For the $[001]_s$ zone, i.e., for $l = 0$, these reduce to

k = even, with h = 4-fold + 2;
k = odd, with h = 4-fold,

and for the $[110]_s$ zone, i.e., for $h = k$, they become

$h = k$ = 4-fold ± 2 l = even;
$h = k$ = 4-fold l = odd;
$h = k$ = 4-fold ± 1 *no extinction.*

This formalism to derive the extinctions is only valid for reflections for which F_o is different from 0, which is the case, except for certain symmetry directions of the chains. For certain reflections F_o may thus become zero due to the stacking of the chains within the layer; reflections may then become extinct for that reason, rather than because of the stacking of the chain layers. In order to take this possibility into account we can write

$$F_o = F_L + F_R \exp(i\pi h),$$

where F_L and F_R are structure factors which still depend on hkl for an L- and R-chain, respectively; they are positioned $\frac{1}{2}\mathbf{a}_s$ apart in the chain layers. Along the [010] zone the chains are viewed along their length axis and due to their symmetry (Fig. 6) we can conclude that $F_L = F_R$ for reflections belonging to the $h0l$ zone.

Similarly, we can write for the [100] zone reflections

$$F_o = F_L + F_R \exp(i\pi k),$$

where again $F_L = F_R$ for reflections belonging to the [100] zone. The factor $\exp(i\pi k)$ takes care of the fact that the tetrahedra which produce the same projected lattice potential in the L- and R-chains are shifted over $\frac{1}{2}\mathbf{b}_s$, due to the presence of a glideline along the chain.

For the formal structure factor of the complete three-dimensional chain arrangement we can thus write for the $h0l$ zone

$$F = [F_L + F_R \exp(i\pi h)] \{1 + \exp[(i\pi/2)(h + 2l)]\}.$$

It is easy to show that spots will only be present for

h = 4-fold, and l = even, or
h = 4-fold + 2, and l = odd.

For the $0kl$ zone we can similarly write

$$F = [F_L + F_R \exp(i\pi k)] \{1 + \exp[(i\pi)(k + l)]\}.$$

It can be shown that F is only different from 0 for reflections for which k = even and l = even. In particular there are no superstructure reflections of the type $h00$ other than those coinciding with basic reflections in agreement with Fig. 6. Nevertheless in the [001] zone pattern (Fig. 5b), such reflections appear, and must be attributed to double diffraction.

These extinction conditions are consistent with those observed in the diffraction patterns of Figs. 5, 6, and 7 and with the reciprocal lattice of Fig. 8.

Acknowledgments

The work in Antwerp has been performed in the framework of a IUAP-48 contract with the Ministry of Science Policy and with the financial support of the Belgian National Science Foundation (NFWO) and the National Impulse Programme on High T_c Superconductivity (SU/03/17). O.M. acknowledges the E.C. Commission for Grant DG XII S/C II*913167.

References

1. Y. Tokura, *Physica C* **185–189,** 174 (1991).
2. C. Greaves and P. R. Slatter, *Physica C* **161,** 245 (1989).
3. P. R. Slater and C. Greaves, *Physica C* **180,** 299 (1991).
4. G. Xiao, M. Z. Cieplak, D. Musser, A. Gavrin, F. H. Streitz, C. L. Chien, J. J. Rhyne, and J. A. Gotaas, *Nature* **332,** 238 (1988).
5. Y. Tokura, J. B. Torrance, T. C. Huang, and A. I. Nazzal, *Phys. Rev. B* **38,** 7156 (1988).
6. G. Roth, P. Adelmann, G. Heger, R. Knitter, and Th. Wolf, *J. de Physique* **1,** 721 (1991).
7. J. T. Vaughey, J. P. Thiel, E. F. Hasty, D. A. Groenke, C. L. Stern, K. L. Poeppelmeier, B. Dabrowski, P. Radaelli, A. W. Mitchel, and D. G. Hinks, *Chem. Mater.* **3,** 935 (1991).
8. Q. Huang, R. J. Cava, A. Santoro, J. J. Krajewski, and W. F. Peck, *Physica C* **193,** 196 (1992).
9. Y. Tokura, T. Arima, H. Takagi, S. Uchida, T. Ishigaki, H. Asano, R. Beyers, A. I. Nazzal, P. Locorre, and J. B. Torrance, *Nature* **342,** 890 (1989).
10. R. Li, Y. Zhu, Y. Qian, and Z. Chen, *Physica C* **176,** 19 (1991).
11. A. Tokiwa, T. Oku, M. Nagoshi, and Y. Syono, *Physica C* **181,** 311 (1991).
12. H. W. Zandbergen, T. Wada, A. Nara, H. Yamauchi, and S. Tanaka, *Physica C* **183,** 149 (1991).
13. A. Nara, T. Wada, A. Ichinose, H. Yamauchi, and S. Tanaka, *Physica C* **184–189,** 599 (1991).
14. R. J. Cava, J. J. Krajewski, H. Takagi, H. W. Zandbergen, R. B. Van Dover, W. F. Peck, Jr., and B. Herssen, *Physica C* **191,** 237 (1992).
15. T. Wada, A. Nara, A. Icinose, H. Yamauchi, and S. Tanaka, *Physica C* **192,** 181 (1992).
16. S. Adachi, O. Inoue, S. Kawashima, H. Adachi, Y. Ichikawa, K. Setsune, and K. Wasa, *Physica C* **168,** 1 (1990).
17. R. J. Cava, R. B. Van Dover, R. Batlogg, J. J. Krajewski, L. F. Schneemeyer, T. Siegrist, B. Henssen, S. H. Chen, W. F. Peck, Jr., and L. W. Rupp, Jr., *Physica C* **184–189,** 180 (1991).
18. B. Dabrovski, P. Radaelli, D. G. Hinks and A. W. Mitchell, J. T. Vaughey, D. A. Groenke, and K. R. Poepelmeier, *Physica C* **193,** 63 (1992).
19. R. M. Hazen, L. W. Finger, R. J. Angel, C. T. Prewitt, N. L. Ross, H. K. Mao, C. G. Hadidiacos, P. H. Hor, R. L. Meng, and C. W. Chu, *Phys. Rev. B* **35,** 7238 (1987).
20. P. M. Grant, R. B. Beyers, E. M. Enger, G. Lim, S. S. P. Parkin, M. L. Ramirez, V. Y. Lee, A. Nazzal, J. E. Vazquez, and R. J. Savoy, *Phys. Rev. B* **35,** 7242 (1987).
21. D. Van Dück, C. Conde-Amiano, and S. Amelinckx, *Phys. Status Solidi A* **58,** 451 (1980).
22. D. Van Dijck, D. Broddin, J. Mahy, and S. Amelinckx, *Phys. Status Solidi A* **103** 357 (1987).
23. O. Milat, G. Van Tendeloo, and S. Amelinckx, to be published.
24. T. Krekels, G. Van Tendeloo, S. Amelinckx, D. M. De Leeuw, and M. De Kraan, *Physica C* **169,** 457 (1990).